NASA TN D-885

11-17
3[illegible]474

TECHNICAL NOTE

D-885

STUDY OF A SOLAR SENSOR FOR USE IN SPACE-VEHICLE ORIENTATION CONTROL SYSTEMS *

By Paul R. Spencer

Langley Research Center
Langley Field, Va.

NATIONAL AERONAUTICS AND SPACE ADMINISTRATION

WASHINGTON June 1961

1A

NATIONAL AERONAUTICS AND SPACE ADMINISTRATION

TECHNICAL NOTE D-885

STUDY OF A SOLAR SENSOR FOR USE IN SPACE-VEHICLE ORIENTATION CONTROL SYSTEMS

By Paul R. Spencer

L
1
3
0
8

SUMMARY

The solar sensor described herein may be used for a variety of space operations requiring solar orientation. The use of silicon solar cells as the sensing elements provides the sensor with sufficient capability to withstand the hazards of a space environment. A method of arranging the cells in a sensor consists simply of mounting them at a large angle to the base. The use of an opaque shield placed between the cells and perpendicular to the base enhances the small-angle sensitivity while adding slightly to the bulk of the sensor. The difference in illumination of these cells as the result of an oblique incidence of the light rays from the reference source causes an electrical error signal which, when used in a battery-bridge circuit, requires a minimum of electrical processing for use in a space-vehicle orientation control system. An error which could occur after prolonged operation of the sensor is that resulting from asymmetrical aging of opposite cells. This could be periodically corrected with a balance potentiometer. A more routine error in the sensor is that produced by reflected earth radiation. This error may be eliminated over a large portion of the operation time by restricting the field of view and, consequently, the capture capability. A more sophisticated method of eliminating this error is to use separate sensors, for capture and fine pointing, along with a switching device.

An experimental model has been constructed and tested to yield an output sensitivity of 1.2 millivolts per second of arc with a load resistance of 1,000 ohms and a reference light source of approximately 1,200 foot-candles delivered at the sensor.

INTRODUCTION

The wide range of space missions requiring solar orientation may be placed in the two broad categories of solar applications and solar research.

The applications include such solar energy converters as parabolic reflecting concentrators and solar-cell batteries which may power either an entire space vehicle or a certain portion of one. In addition to providing an economical and accessible source of energy for long-time space operations, the solar disk is a convenient beacon for space navigation. Still another solar property which may someday be used is the radiation pressure for which solar sails have been proposed as low-thrust devices.

The solar research projects which are of immediate concern include a study of the solar energy spectrum in bands that are inaccessible below the earth's atmosphere. In addition to satellite insolation measurement and control, a solar-oriented satellite could monitor the solar constant to furnish invaluable data for terrestrial heat-balance studies. A solar-oriented telescope could yield information on sunspots, flares, or other aspects of the solar atmosphere.

A few sensors have been designed prior to the present investigation and although these existing designs are adequate for some types of experiments, more stringent demands must be met in regard to prolonged reliability and pointing sensitivity. The solar sensor proposed in this paper is offered as an attempt to meet these demands. In addition to reliability and pointing sensitivity, consideration was given to other requirements such as initial acquisition of the solar disk, endurance, weight, power consumption, and economy and ease of fabrication.

It is the purpose of this paper to describe an approach toward satisfying the existing requirement for a highly accurate, "work-horse" solar sensor with no delicate or moving parts.

SYMBOLS

A	area of sunlit portion of projected earth
A'	special case of A
a	semimajor axis of ellipse formed by projecting sunlit region of earth
b	semiminor axis of ellipse formed by projecting sunlit region of earth
C	illumination per unit area on flat surface located in vicinity of cell and normal to illuminating source, watts/sq in.
F	fractional decrease of sunlit area

H	length of opaque shield
h	height of satellite above surface of earth
I	illumination of solar cell for arbitrary inclination to illuminating source, ft-candles
ΔI	difference in illumination between opposite cells
$k = R_E/(R_E + h)$	
l	length of solar cell
N	surface normal
O	center of reflected sunlight
q	amount of cell's length shaded by opaque shield
R_E	radius of earth
S	area of cell under illumination
w	width of solar cell
x	distance from center of illumination of earth-reflected sunlight to line from center of earth to satellite
α	angle between solar cell and base of solar sensor
β	angle of incidence
β_d	angle of incidence of direct sunlight on cell
β_r	angle of incidence of reflected sunlight on cell
γ	half of total capture angle of solar sensor
δ	angle formed by line from center of earth to satellite and earth tangent passing through satellite
η	angle of solar sensor error caused by reflected sunlight
θ	angle between solar sensor base normal and direction of solar radiation
ϕ	angle between lines from satellite to center of earth and to center of reflected sunlight

L
1
3
0
8

ψ angle formed by line from center of earth to satellite and earth-sun line of centers

ψ' angle between earth-sun line of centers and line from satellite to center of reflected sunlight

Subscripts:

1 cell 1

2 cell 2

b base of sensor

crit value of independent variable for which functional relationship changes

E earth

max maximum value

S sun

L 1308

DESCRIPTION

The purpose of any solar sensor is to provide a space-vehicle control system with an electrical signal that is proportional to the angle of incidence between the sun and a reference axis on the space vehicle to be oriented. The control system may then amplify this signal to obtain the magnitude and sense of reaction torque required for vehicle alinement.

An angular detection device like the solar sensor must be capable of performing two separate functions: It should be able to capture the reference source of radiation and, once acquired, it should hold this source within a narrow confine. The capture phase may be accomplished by a coarse sensor, while the second phase requires a fine sensor. These may be either separate units or combined as is the sensor presented herein.

To simplify the discussion presented in this report, only single-degree-of-freedom orientation is considered. To obtain another degree of freedom, all that is necessary is to introduce a second set of cells on the same base but rotated orthogonally to the first set.

Figure 1 shows part of the photometrical principle of operation for the sensor described in this report. The basic operating principle is that the illumination of a flat surface is directly proportional to the cosine of the angle of incidence.

For the condition

$$0 < \theta < 90^{\circ} - \alpha$$

the illumination of cell 1 is given by

$$I_1 = I_{max} \cos \beta_1 \qquad (\beta_1 = \alpha + \theta)$$

and likewise for cell 2

$$I_2 = I_{max} \cos \beta_2 \qquad (\beta_2 = \alpha - \theta)$$

where I_{max} is the illumination of cell 2 when

$$\theta = \alpha$$

It may be seen that for the case when the incident solar radiation is parallel to N_B (the case when $\theta = 0$) the cells are equally illuminated and produce equal potentials if their electrical characteristics are matched. Mismatched cells may be used by placing a resistor in series with the stronger cell. This resistor may also be adjusted to point the sensor at any desired angle to the sun. The cells are connected in a battery-bridge circuit shown in figure 2. When the solar sensor is alined toward the center of the solar disk, there will be no current through the center of the bridge, which is actually the control system. If, however, the incident radiation forms an angle θ with the sensor normal N_B, then the more illuminated cell will produce an electrical signal through the center of the bridge. This signal will increase in intensity with increasing error angle, θ, and will reach a maximum when the incident radiation becomes perpendicular to the more illuminated cell. It should be noted that when θ reverses in sense, the signal to the control system similarly reverses polarity.

The sensor of figure 1 could be used as a coarse sensor for somewhat uncritical types of orientation applications. If it is assumed that the output of a solar cell is linear, the electrical output would

be directly proportional to the difference in cell illumination, and the output of this type of coarse sensor would be that shown on figure 3. The linearity assumption is correct only up to certain error angles as will be shown later in this report. Figure 3 also shows the effect of varying α, the angle of inclination of the solar cell with respect to the sensor base. The complete equations for the curves shown are

when both cells are illuminated:

$$\Delta I = I_{max}\left[\cos(\alpha - \theta) - \cos(\alpha + \theta)\right] \qquad (0 < \theta < 90^\circ - \alpha)$$

when one cell is illuminated:

$$\Delta I = I_{max} \cos(\alpha - \theta) \qquad (90^\circ - \alpha < \theta < 90^\circ + \alpha)$$

and when neither cell is illuminated:

$$\Delta I = 0 \qquad (\theta > 90^\circ + \alpha)$$

With a slight increase in bulk, a significant gain in precision for the previously described sensor can be realized through the addition of an opaque shield at the apex as is shown in figure 4. It may be seen, qualitatively at least, that the shadow cast by the shield on cell 1 will cause a greater change in sensor output for small error angles. For most applications, the angle made by the solar cells with the base should be large. An inclination angle α of 80° was chosen for the graph in figure 5. This angle produced both a steep slope and a wide linear range. Figure 5 shows quantitatively the advantage gained by the addition of a reasonable size shield (5 inch). If the shield is made reflecting, a slight increase over the output shown is realized. It should be noted that there is no loss of wide-angle capture capability by the addition of a shield, thus providing a sensor which has both wide-angle capture capability and a high sensitivity for small angles. The method of obtaining figure 5 is presented in appendix A. The effect of changing the length of the opaque shield for small error angles is seen in equation (A1). From the linear relationship of H and ΔI, it is seen that the optimum length of the shield is a more or less arbitrary parameter which can be decided upon only after consideration is given to structural factors, mission requirements, and space available for the sensor. A 5-inch shield was used in the calculations as a reasonable balance between compactness and sensitivity.

L 1308

Still another quantity subject to change is the geometric shape of the cell which may be used to a limited extent to control the slope of the curve for small angles. For most purposes a smooth maximum slope is desired, which led to the use of rectangular cells in this discussion.

The calculations showing the effect of various sensor parameters have some slight error since they do not take account of the penumbra due to the finite angle (about $1/2^{o}$) subtended by the solar disk.

L
1
3
0
8

ENVIRONMENT

An important requirement for the solar sensor is that it be capable of reliable, long-time operation in the environment of space. Among the hazards likely to be encountered are severe particle and electromagnetic radiation, vacuum, and micrometeor bombardment.

An investigation of photosensitive devices leads to the selection of silicon solar cells as the photosensitors that would provide sustained reliable operation in a space environment. There are several reasons for preferring these over other photosensitive devices, the most significant of which is the high ratio of electrical power output to incident solar power. This conversion efficiency of 11 percent is better by a factor of 10 than that of other converting devices (ref. 1). Furthermore, the silicon spectral-response curve compares very favorably with respect to the solar output as may be seen in figure 6 (ref. 1). This relatively high conversion ability minimizes the equipment required to process the electrical signal. This equipment would introduce additional weight and failure possibility.

Silicon solar cells have proven capable of reliable operation in a space environment. This was accomplished by the first successful Vanguard satellite, 1958 Beta, whose cells have been operating for an extended period. By the same experiment their ruggedness has proven satisfactory.

In addition to this satellite experiment, some laboratory tests on the effects of radiation upon silicon solar cells were performed (ref. 2). The test cells were subjected to ultraviolet light, X-rays, gamma rays, electrons, protons, and alpha particles, both in air and in vacuum. Based on knowledge of space radiation prior to the discovery of the Van Allen belt, expected lifetimes (75 percent original output) were estimated at 1.4×10^{5} years. Depending upon the composition of this belt, this figure may have to be reduced by as much as four orders of magnitude. More reliable radiation-damage predictions must await more complete data concerning the nature of the Van Allen belt and other deleterious phenomena such as solar proton streams.

Another hazard to the solar sensor is the damage which might be caused by micrometeorite erosion and puncture. However, present data indicate that this problem is less serious than is radiation damage (ref. 3). In order to protect the silicon cells from the sandblasting effects of micrometeorites, windows of highly resistant fused silica may be provided. Although these have favorable mechanical properties, up to 20 percent of the transmitted energy may still be lost by the sandblasting effects (ref. 4).

If a satellite experiment using the sensor requires prolonged pointing with reasonable accuracy, there must be provided a means to correct for aging, which is the decrease in voltage that occurs with time. This decrease would result in a drift of the zero position of the sensor, if the aging did not occur symmetrically for the cells.

L
1
3
0
8

An approach toward compensating for the drift, when this becomes necessary, is seen schematically in figure 7. A bright a-c operated light, mounted on the forward end of the sensor, is flashed on the silicon solar cells at widely separated time intervals by reflecting the beam from a half-silvered mirror mounted in front of the flashing lamp. The a-c component due to any unbalance of the cell output, can then be separated, amplified, and used to control servomechanically a potentiometer which would change the balance of the bridge to its original zero position.

Although this method introduces moving parts which invite system failure, should the compensator fail it would remain on its last setting, thereby causing no greater total error than would result from asymmetrical aging after failure of the compensator.

If one sensor is to be used for the dual purpose of initial capture and fine sensing, then a significant error which must be taken into consideration is that due to sunlight reflected from the earth. Since the solar sensor has an extremely wide field of view, it is capable of viewing two light sources simultaneously. When this occurs, the sensor would tend to point the control system away from the reference source in the direction of the interfering source, the angular error being related to the angular separation of the two sources and their relative intensities.

If a complete spherical field of view is assumed, solar cells being back to back, then the error caused by reflected earth radiation is seen in figure 8, which is for the orbit passing through the earth-sun line of centers. The problem geometry and calculations appear in appendix B for a 360° capture angle, this angle being defined as the maximum total angle through which the sensor may be rotated while being continuously

illuminated by a point light source. For a smaller capture angle the error is somewhat less as is seen in figure 9, and a method of eliminating this error for a large portion of the time suggests itself. The extremely wide capture angle may be reduced by adding an opaque cone to the sensor as is shown in figure 10. The geometry of this figure may be applied to determine the value of ψ for which the sensor can no longer view the earth. Since

$$\sin \delta = \frac{R_E}{R_E + h}$$

L
1
3
0
8

and since

$$\psi + \delta + \gamma = 180^\circ$$

then

$$\psi = 180^\circ - \sin^{-1} \frac{R_E}{R_E + h} - \gamma$$

This last equation was used to establish in figure 9 the values for which the reflected sunlight causes no error, when the solar sensor is at an altitude of 300 miles.

Figure 11 shows a technique which may be used to eliminate rather than restrict the reflected-sunlight error. This consists of placing a concentric sensor within a larger hollow sensor with a solar cell to switch off the coarse sensor only when the solar constant is received by the silicon cell switch. Initial capture is attained in the same manner already mentioned; but when the silicon cell switch is actuated by the solar radiation, the inner sensor solely operates the control system and has no reflected-sunlight error due to its restricted field of view. The anticipated drawback of this method is that the switching is done by a switching transistor or a relay, both of which appear to have drawbacks.

The switching transistor has a cut-off current that would approach in magnitude the level of the sensor output signal for very fine pointing. The relay, on the other hand, would introduce a moving part, tending to defeat the major advantage of this sensor - reliability of sustained operation. Should neither of these two methods prove feasible, then it would be desirable to decrease the sensitivity of the external sensor

of figure 11 and connect the sensors in parallel. Once capture is attained the interior sensor exerts a greater influence on the signal so that the reflected-sunlight error is at least diminished.

It is believed that other extraneous light sources will be of a much lesser magnitude than will reflected sunlight. For example, the moon produces five or six orders of magnitude less than the solar constant due to its lower albedo and, even more important, due to its small angular size. The effects of starlight will be negligible to the sensor.

L
1
3
0
8

APPARATUS, MEASUREMENTS, AND RESULTS

The experimental solar sensor presented in figure 12 was constructed for use on a single-degree-of-freedom platform which is mounted on an air bearing and oriented toward a bright light source which simulates the sun. The large-angle calibration curve of figure 13 was obtained by rotating the sensor at various angles to a collimated beam emitted by the aircraft landing lamp shown in figure 14. This photograph also shows the collimating tube used in conjunction with the lamp. The reason for the knee appearing in figure 13 is that the solar cells used attained rapid saturation as may be seen from the saturation curve of figure 15.

By using the same light source, the small-angle calibration curve of figure 16 was obtained with the aid of the equipment shown in figure 14. Very small changes in incidence angle could be obtained with this equipment which consists of a sturdy I-beam supported on one end by a vertical torsion bar with a micrometer drive screw on the unsupported end. Very small displacements of the movable end produce a minute rotation of the supported end about the vertical torsion bar. These small displacements were read on a microscope reticle attached to the movable end. Due to the extremely high ratio of I-beam flexural rigidity to support-bar torsional rigidity, the flexural rigidity introduces virtually no error. Any lateral motions of the supported end which may have occurred could not be detected with a microscope, which indicated that no significant error occurred in that respect. The microscope reticle consisting of 100 lines per millimeter could be read to the nearest 1/2 line, an accuracy which would correspond to about 1 second of arc rotation of the sensor.

The results of this small-angle calibration of the solar sensor with a load resistance of 1,000 ohms and with an illumination of 1,200 foot-candles are presented in figure 16. The linearity of the calibration curve for very small angles is in agreement with the theory, and is very desirable for processing the electrical signal. The sensitivity obtained is shown on the curve as a sensor output of

1.2 millivolts for 1 second arc. With moderate amplification this signal should be sufficient to operate a control system to a high degree of accuracy.

CONCLUSIONS AND RECOMMENDATIONS

Although further developmental work should be performed on the solar sensor presented herein, the following conclusions may be drawn from this study:

1. A passive sensor is feasible with reasonable dimensions, no power consumption, broad-angle capture capability, and high sensitivity.

2. The use of an opaque shield enhances the sensitivity of the sensor.

3. Silicon solar cells are recommended because of their high conversion efficiency.

4. It will be desirable to reduce the effects of reflected sunlight from a nearby planetary body either by shielding the sensor or by incorporating a two-level sensor.

5. A sensor was constructed and ground-tested to yield a sensitivity of 1.2 millivolts per second of arc.

6. In order to design a method of correcting long-term drift in the solar sensor, more data should be obtained on the extent of silicon cell output decrease after prolonged exposure to the space environment.

Langley Research Center,
National Aeronautics and Space Administration,
Langley Field, Va., March 21, 1961.

APPENDIX A

THEORETICAL PERFORMANCE OF SOLAR SENSOR WITH OPAQUE SHIELD

The discussion presented in this appendix refers to figure 4.

The illumination of either cell may be expressed as

$$I = Cw(l - q) \cos \beta$$

L
1
3
0
8

where

C illumination per unit area on a flat surface located in the vicinity of the cell and normal to the illuminating source

w width of cell

l length of cell

q amount of cell's length shaded by shield

β angle of incidence

The area of cell 1 under illumination is

$$S_1 = w(l - q)$$

From the geometry of figure 4

$$q = \frac{H \sin \theta}{\cos(\alpha + \theta)}$$

so that

$$S_1 = w\left[l - \frac{H \sin \theta}{\cos(\alpha + \theta)}\right]$$

Since the illumination of cell 1 diminishes as the cosine of the angle of incidence, this illumination is

$$I_1 = Cw \cos(\alpha + \theta)\left[l - \frac{H \sin \theta}{\cos(\alpha + \theta)} \right]$$

Similarly for cell 2

$$I_2 = Cwl \cos(\alpha - \theta)$$

Subtraction yields

$$I_2 - I_1 = \Delta I = Cw\left[l \cos(\alpha - \theta) - l \cos(\alpha + \theta) + H \sin \theta \right] \qquad (A1)$$

L
1
3
0
8

for the condition

$$0 \leqq \theta \leqq \theta_{crit}$$

where θ_{crit} is the value of θ for which cell 1 becomes completely shaded and is given by

$$\theta_{crit} = \tan^{-1} \frac{\cos \alpha}{H + \sin \alpha}$$

For larger values of θ

$$\Delta I = Cwl \cos(\alpha - \theta) \qquad (A2)$$

It may be noted that the special case of equation (A1) which occurs when $H = 0$ is used to obtain the coarse sensor performance shown in figure 3.

APPENDIX B

ERROR CAUSED BY EARTH-REFLECTED SUNLIGHT

The problem geometries of figures 17 to 20 will be used to determine the error angle η which will be introduced in a solar sensor as a result of viewing reflected earth radiation as an unwanted source of illumination. For a given satellite altitude, this error angle shall be described as a function of ψ, the angle between the line from the satellite to the center of the earth and the earth-sun line of centers. This may be done because the earth-sun line of centers provides an axis of symmetry for the problem.

If the solar disk were the only source of illumination supplied to the sensor, it could be considered as a point source located in the center of the disk and having an intensity equal to the extended source. When the sensor is illuminated by two such sources, in general, it will not point toward the center of either, but will point to a location somewhere between the sources determined by the relative source intensities and their angular separation.

From figure 17 is seen the condition which establishes the balance of solar and reflected-earth radiation on the sensor when two point sources are assumed. It is also assumed that α is close enough to 90° so that one cell views only the sun and the other views only the earth.

$$I_S \cos \beta_d = I_E \cos \beta_r \tag{B1}$$

where

I_S cell illumination from point source sun

I_E cell illumination from point source reflection of sunlight from the earth

β_d angle of incidence of direct sunlight on cell

β_r angle of incidence of reflected sunlight on cell

From the geometry of figure 17

$$\beta_d = \alpha - \eta$$

and

$$\beta_r = \alpha + \psi' + \eta - 180^\circ$$

Substituting these equations in equation (B1) gives

$$I_S \cos(\alpha - \eta) = -I_E \cos\left[(\alpha + \psi') + \eta\right]$$

L
1
3
0
8

which may be expanded by suitable trigonometric identities to yield

$$\eta = \tan^{-1} \frac{I_E \cos(\alpha + \psi') + I_S \cos \alpha}{I_E \sin(\alpha + \psi') - I_S \sin \alpha} \tag{B2}$$

When total spherical capture capability is obtained $\alpha = 90^\circ$ and equation (B2) becomes

$$\eta = \tan^{-1} \frac{I_E \sin \psi'}{I_S - I_E \cos \psi'} \tag{B2a}$$

This is the case shown in figure 8.

The reflected sunlight presents separate aspects for the following conditions:

1. $0 \leqq \psi \leqq \psi_{crit}$
2. $\psi_{crit} < \psi < 180^\circ - \psi_{crit}$
3. $180^\circ - \psi_{crit} \leqq \psi \leqq 180^\circ$

It is not necessary to describe the other two quadrants because of symmetry. For the first condition, the sunlit portion of the earth is viewed as a circle of radius a. The second condition, the one appearing in figure 18, presents the sunlight region as a semicircle of radius a to the right of JK a semiellipse with semimajor and semiminor axes of a and b, respectively, to the left of JK where b is considered positive to the left of JK and negative to the right. When the third condition exists, the solar sensor receives no reflected sunlight. The second condition is the most general case, being reducible to the first

condition when $b = a$, $x = 0$, and $\psi = \psi'$. The second case is therefore the one for which the argument shall be developed.

For the first condition, it was assumed that the earth follows Lambert's law for a flat diffuse surface and decreases in intensity with the cosine of the angle of incidence. The radiation viewed as a function of the angle of incidence becomes

$$I_E = I_{E,max} \cos \psi \qquad (0 \leq \psi \leq \psi_{crit}) \qquad (B3)$$

L 1 3 0 8

where $I_{E,max}$ is the radiation viewed when $\psi = 0$ and is given as (ref. 5)

$$I_{E,max} = 2(\text{solar constant})(\text{earth's albedo})\left[1 - (1 - k^2)^{1/2}\right]$$

where $k = \dfrac{R_E}{(R_E + h)}$

If $h = 300$ miles and 0.36 is the earth's albedo, then $I_{E,max}$ becomes

$$I_{E,max} = 0.455 \text{ (solar constant)} \qquad (B4)$$

From the geometry of figure 18

$$a = \frac{R_E}{R_E + h}\sqrt{(R_E + h)^2 - R_E^2} \qquad (B5)$$

and

$$b = R_E \cos \psi \qquad (\psi > \psi_{crit}) \qquad (B6a)$$

$$b = a \qquad (\psi < \psi_{crit}) \qquad (B6b)$$

If A is the area of sunlit portion viewed, then

$$A = \frac{1}{2} \pi a(a + b)$$

For the second condition, the one shown in figure 18, I_E diminishes more rapidly than the first condition because both the area viewed and the cosine of the angle of incidence diminish. For the second condition

$$I_E = I_{E,max} F \cos \beta \qquad (\psi_{crit} < \psi < 180^\circ - \psi_{crit}) \qquad (B7)$$

where F is the fractional decrease in sunlit area and β is the angle of incidence for this second condition. If A' is defined as the area viewed during the first condition, then

L
1
3
0
8

$$F = \frac{A}{A'}$$

and since

$$A' = \pi a^2$$

then

$$F = \frac{a + b}{2a} \qquad (B8)$$

From the geometry of figure 19

$$\sin \gamma = \frac{x}{R_E}$$

and

$$\beta = \psi - \gamma$$

which may be combined to give

$$\beta = \psi - \sin^{-1} \frac{x}{R_E} \qquad (B9)$$

From figure 18 it is apparent by symmetry that the center of reflected sunlight O is located along the line FG and the further assumption is made that this center lies midway between F and G to produce the simple relationship

$$x = \frac{1}{2}(a - b) \qquad (B10)$$

Rewriting equation (B3) and substituting equations (B8), (B9), and (B10) into equation (B7) gives

$$I_E = 0.455\, C_S \cos\psi \qquad (0 \leqq \psi \leqq \psi_{crit})$$

$$= 0.455\, C_S \frac{a+b}{2a} \cos\left(\psi - \sin^{-1}\frac{a-b}{2R_E}\right) \qquad (\psi_{crit} < \psi < 180^\circ - \psi_{crit}) \tag{B11}$$

To determine ψ' as a function of ψ, reference is made to figure 18 from which may be seen that

$$\psi' = \phi + \psi \tag{B12}$$

L 1 3 0 8

From figure 20

$$\phi = \tan^{-1}\frac{x}{\left[(R_E + h) - \sqrt{R_E^2 - x^2}\right]}$$

for the condition

$$\psi_{crit} < \psi < 180^\circ - \psi_{crit}$$

but for the condition

$$0 \leqq \psi \leqq \psi_{crit}$$

$$\phi = 0 \tag{B13}$$

as is seen in figure 18 when x approaches zero and b approaches a.

In summary, the equations used to obtain figure 9 are

equation (B2a):

$$\eta = \tan^{-1}\frac{I_E \sin\psi'}{I_S - I_E \cos\psi'}$$

equation (B3):

$$I_E = I_{E,max} \cos\psi \qquad (0 \leqq \psi \leqq \psi_{crit})$$

equation (B7):

$$I_E = I_{E,max} F \cos \beta \qquad (\psi_{crit} < \psi < 180^\circ - \psi_{crit})$$

equation (B4):

$$I_{E,max} = 0.455\ I_S \qquad \begin{pmatrix} \text{altitude, 300 miles;} \\ I_S, \text{ solar constant} \end{pmatrix}$$

L
1
3
0
8

equation (B8):

$$F = \frac{a + b}{2a}$$

where (eq. (B5))

$$a = \frac{R_E}{R_E + h}\sqrt{(R_E + h)^2 - R_E^2}$$

and (eq. (B6a))

$$b = R_E \cos \psi$$

equation (B9):

$$\beta = \psi - \sin^{-1} \frac{x}{R_E}$$

where (eq. (B10))

$$x = \frac{1}{2}(a - b)$$

REFERENCES

1. Pearson, G. L.: Electricity From the Sun. Proc. World Symposium on Applied Solar Energy (Phoenix, Ariz.), Nov. 1-5, 1955, pp. 281-288.

2. Loferski, J. J., and Rappaport, P.: The Effect of Radiation on Silicon Solar-Energy Converters. RCA Review, vol. XIX, no. 4, Dec. 1958, pp. 536-554.

3. Whipple, Fred L.: The Meteoritic Risk to Space Vehicles. [Preprint] 499-57, Am. Rocket Soc., Oct. 1957.

4. Zahl, Harold A., and Ziegler, Hans K.: Power Sources for Satellites and Space Vehicles. Solar Energy, vol. IV, no. 1, Jan. 1960, pp. 32-38.

5. Wood, George P., and Carter, Arlen F.: Predicted Characteristics of an Inflatable Aluminized-Plastic Spherical Earth Satellite With Regard to Temperature, Visibility, Reflection of Radar Waves, and Protection From Ultraviolet Radiation. NASA TN D-115, 1959.

L-1308

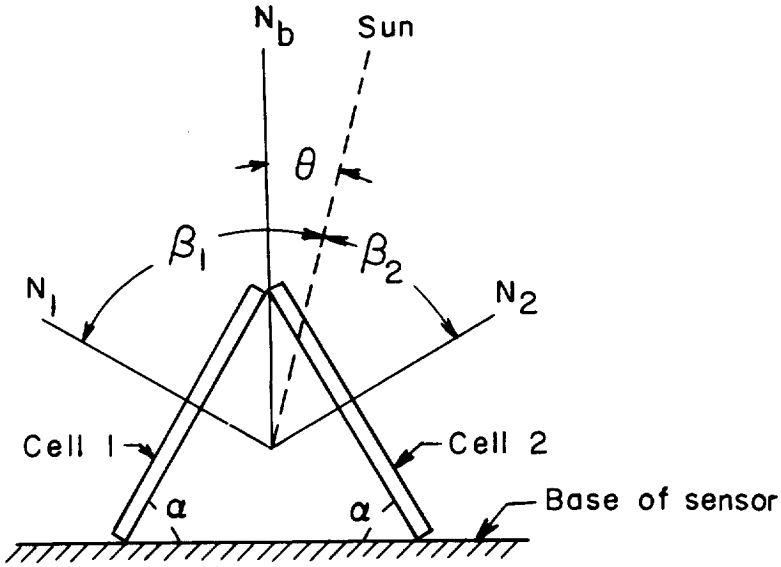

Figure 1.- Photometrical principle of operation.

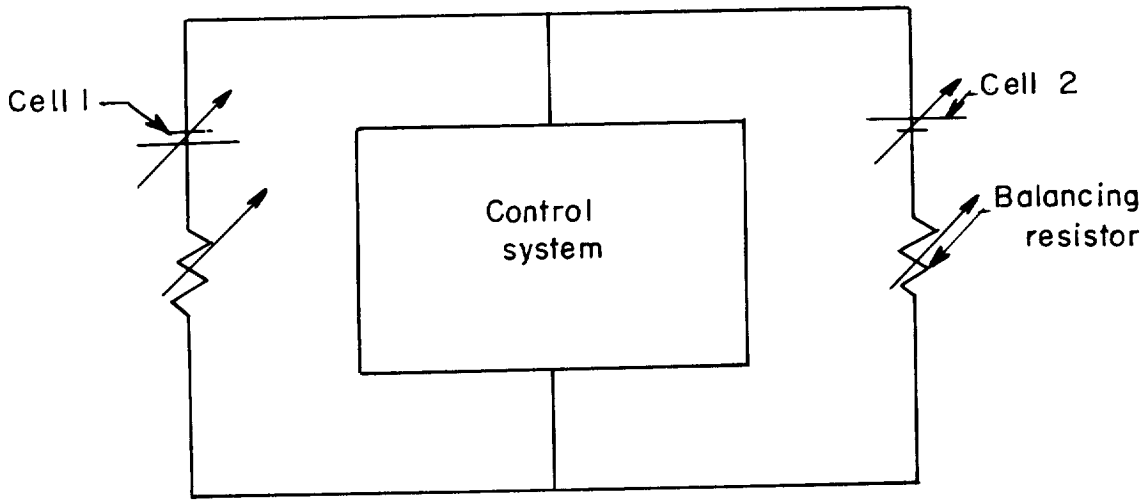

Figure 2.- Electrical principle of operation.

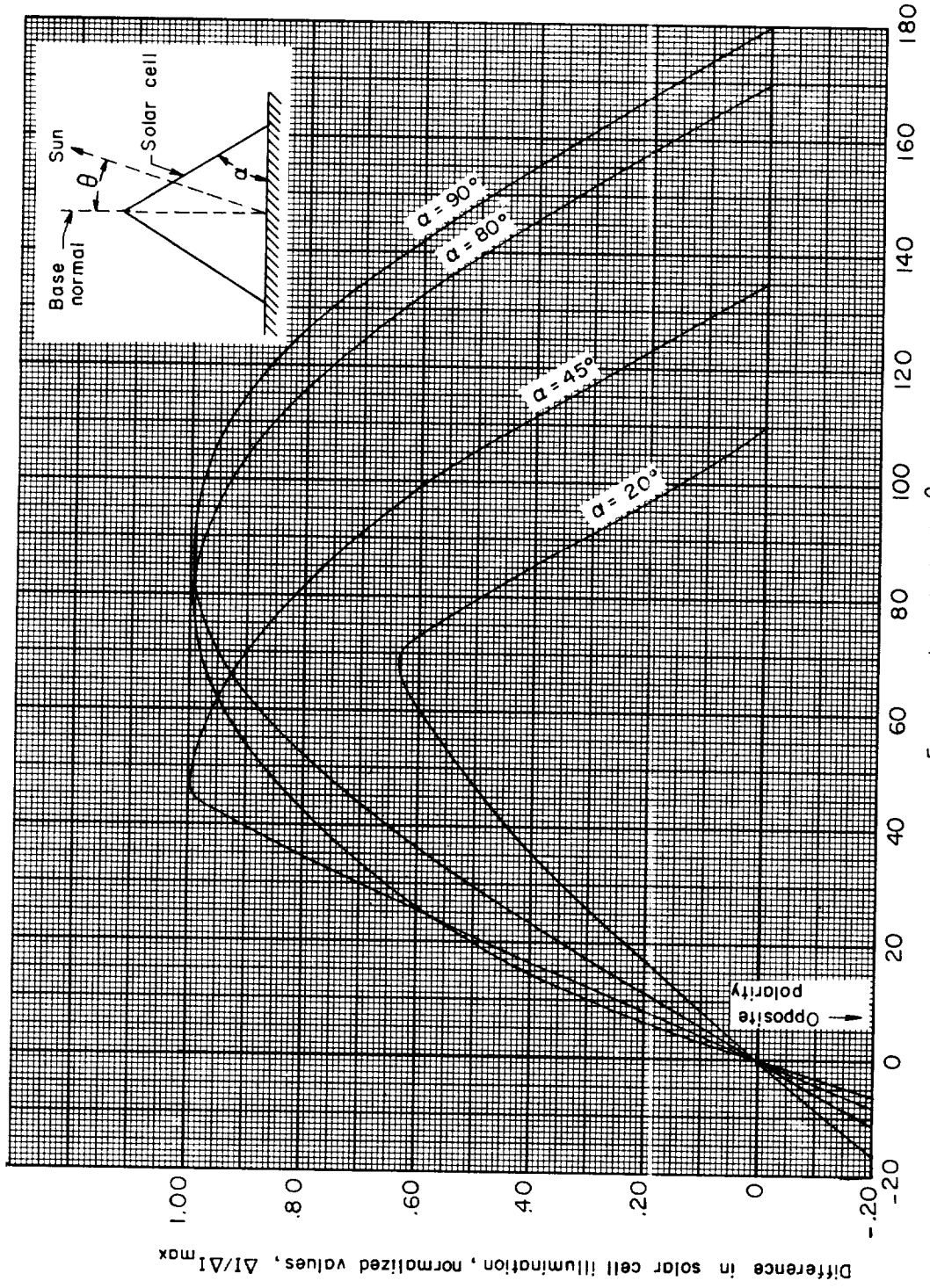

Figure 3.- Output of coarse sensor for various angles of solar cell inclination.

L-1308

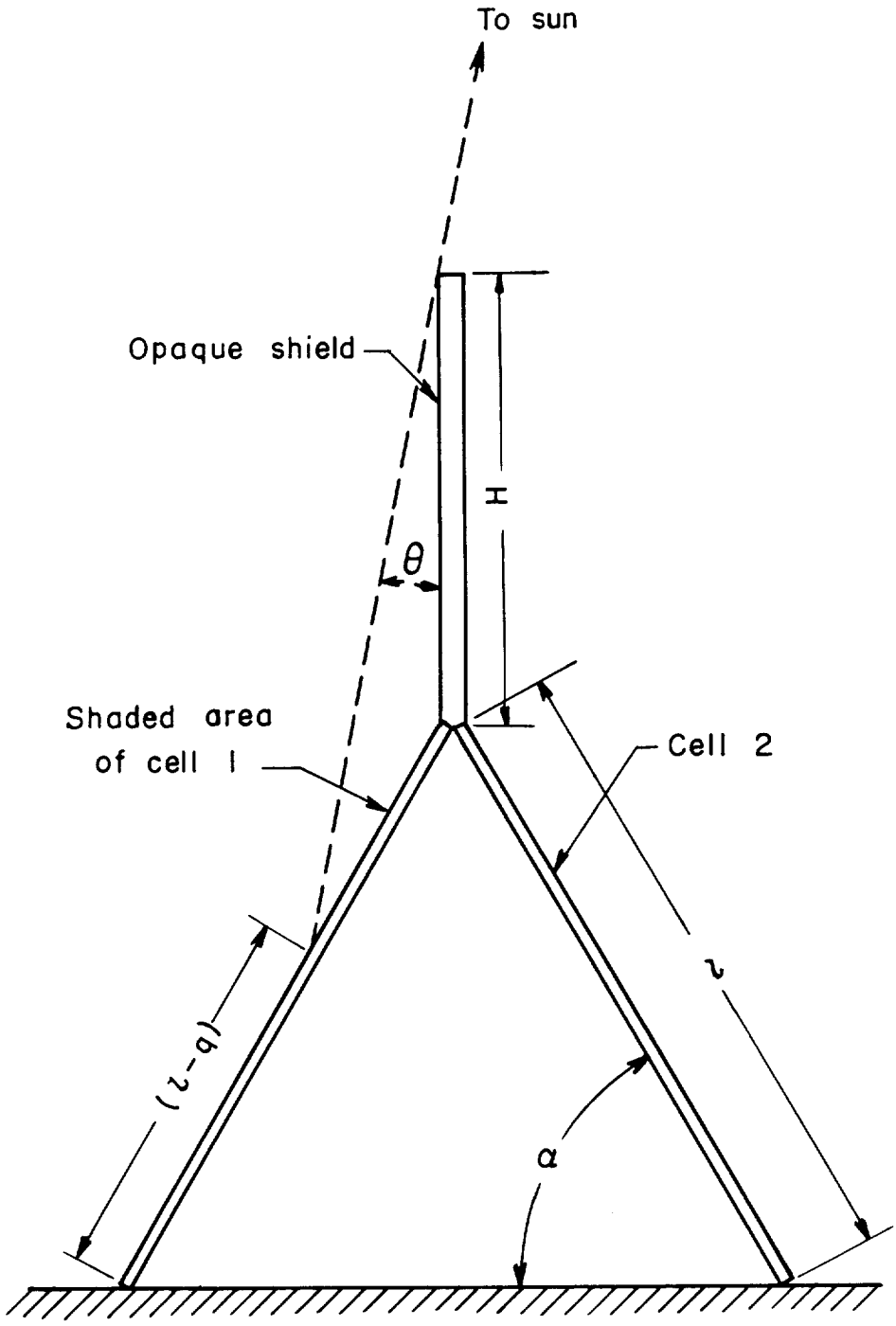

Figure 4.- Shading effect of opaque shield. Dimensions are shown for the calculations of appendix A.

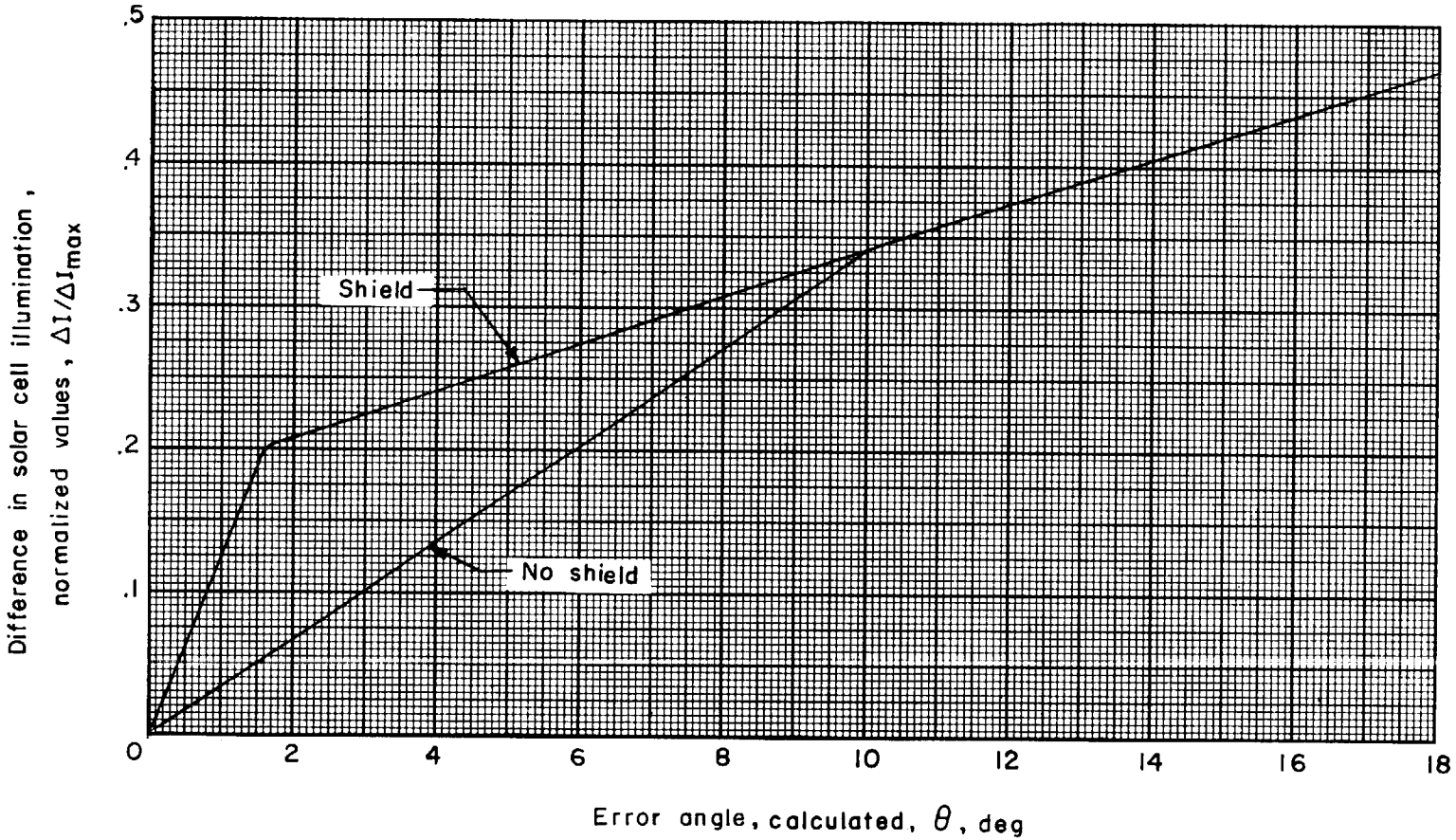

Figure 5.- Effect of shield. $\alpha = 80^{\circ}$; shield length, 5 inches; solar cells, 1 inch square.

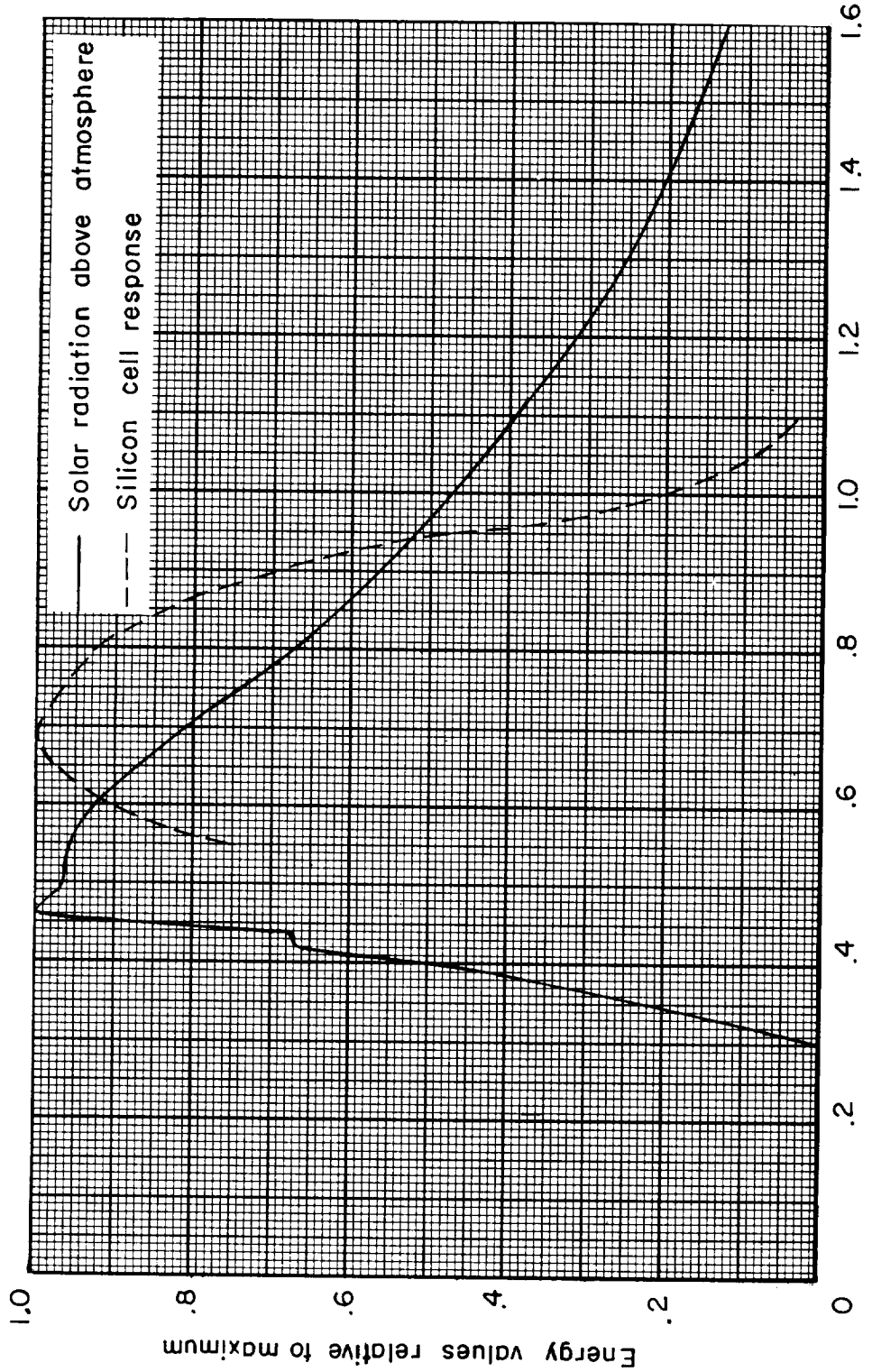

Figure 6.- Solar-radiation curve and spectral response of silicon cell.

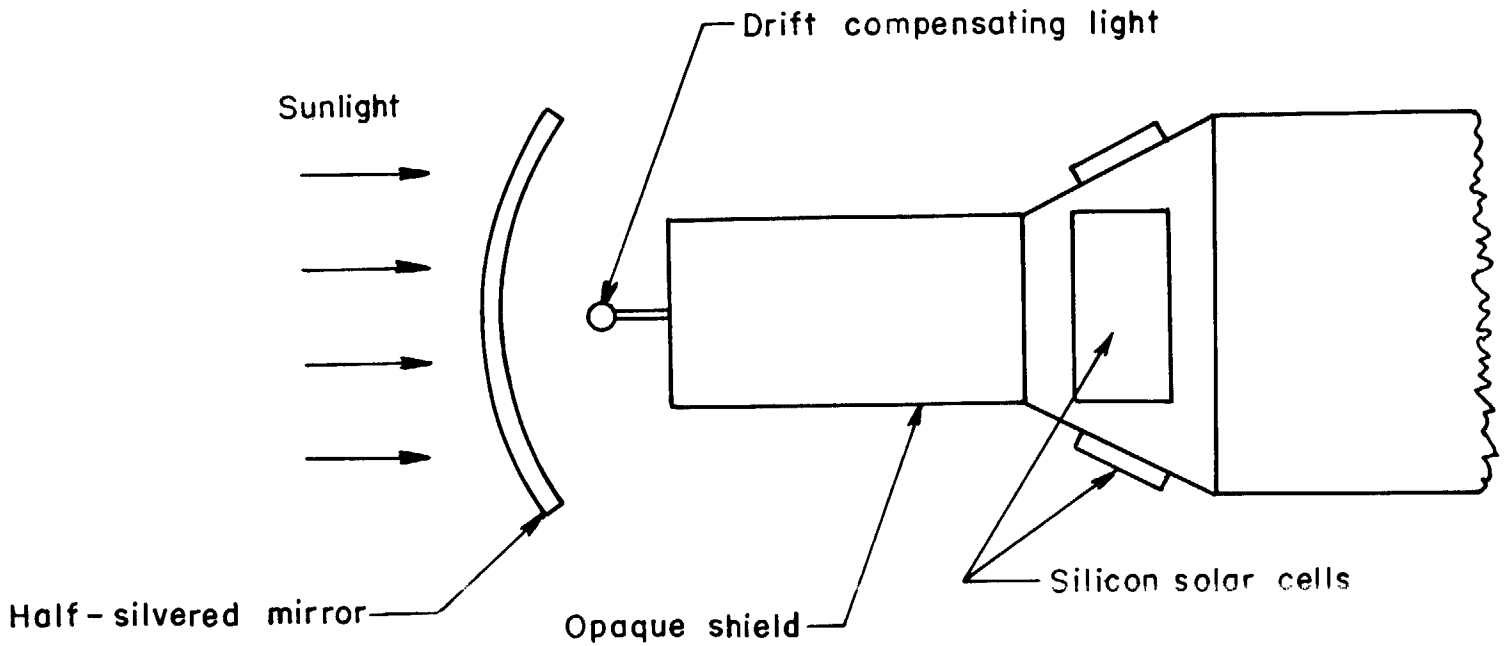

Figure 7.- Method of compensation for unequal aging of cells.

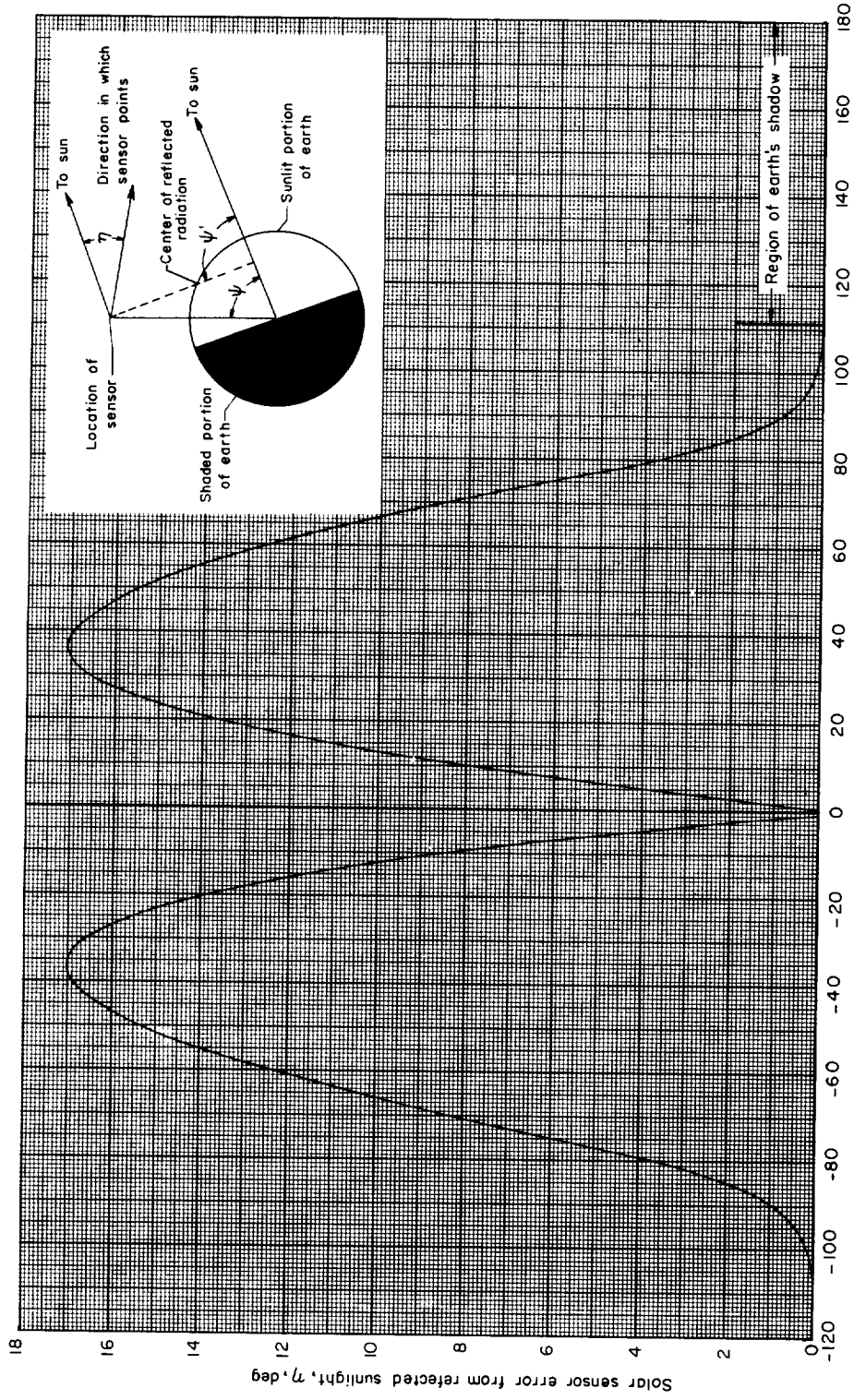

Figure 8.- Solar sensor error with complete capture capability at an altitude of 300 miles.

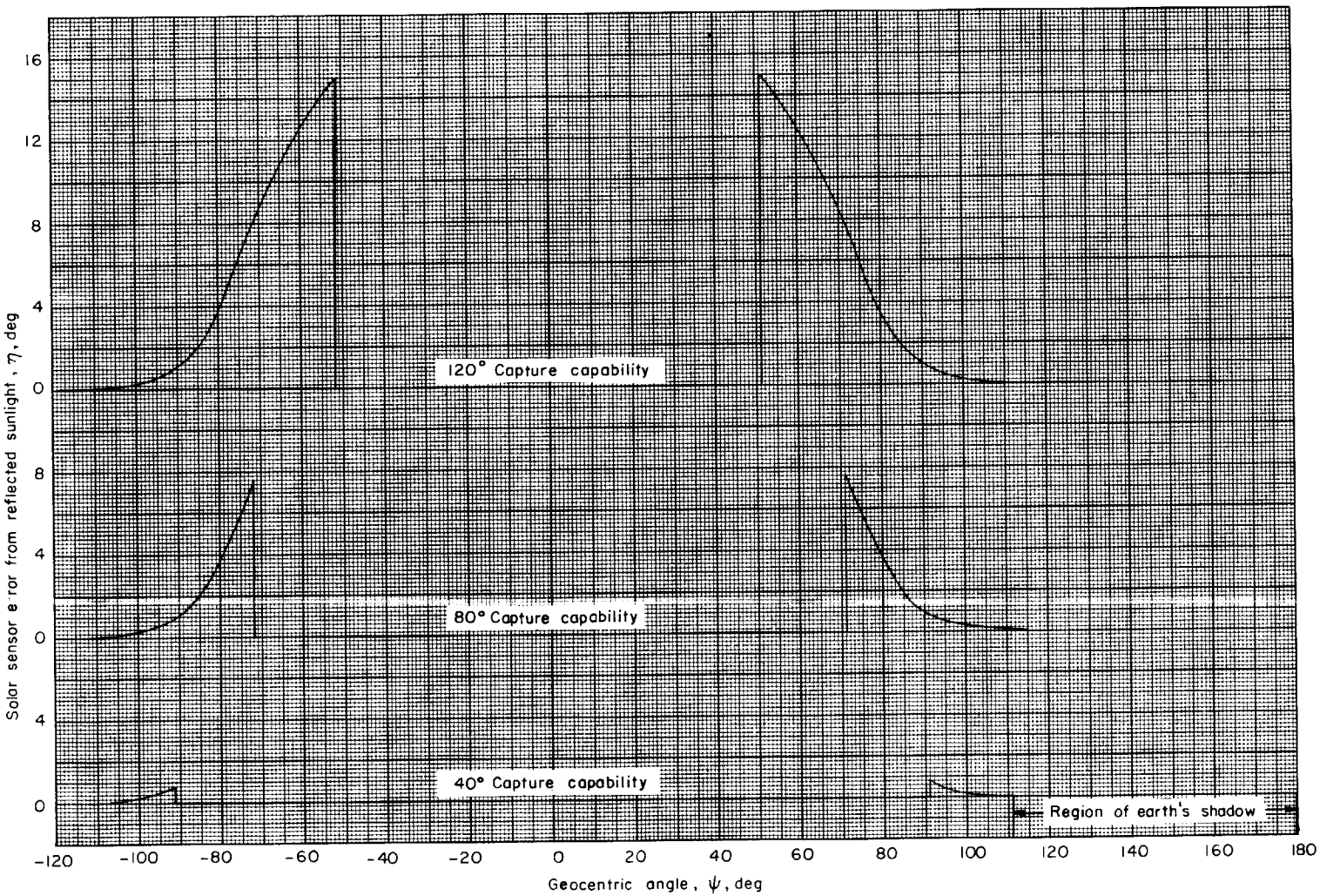

Figure 9.- Solar sensor error for various capture capabilities at an altitude of 300 miles.

L-1308

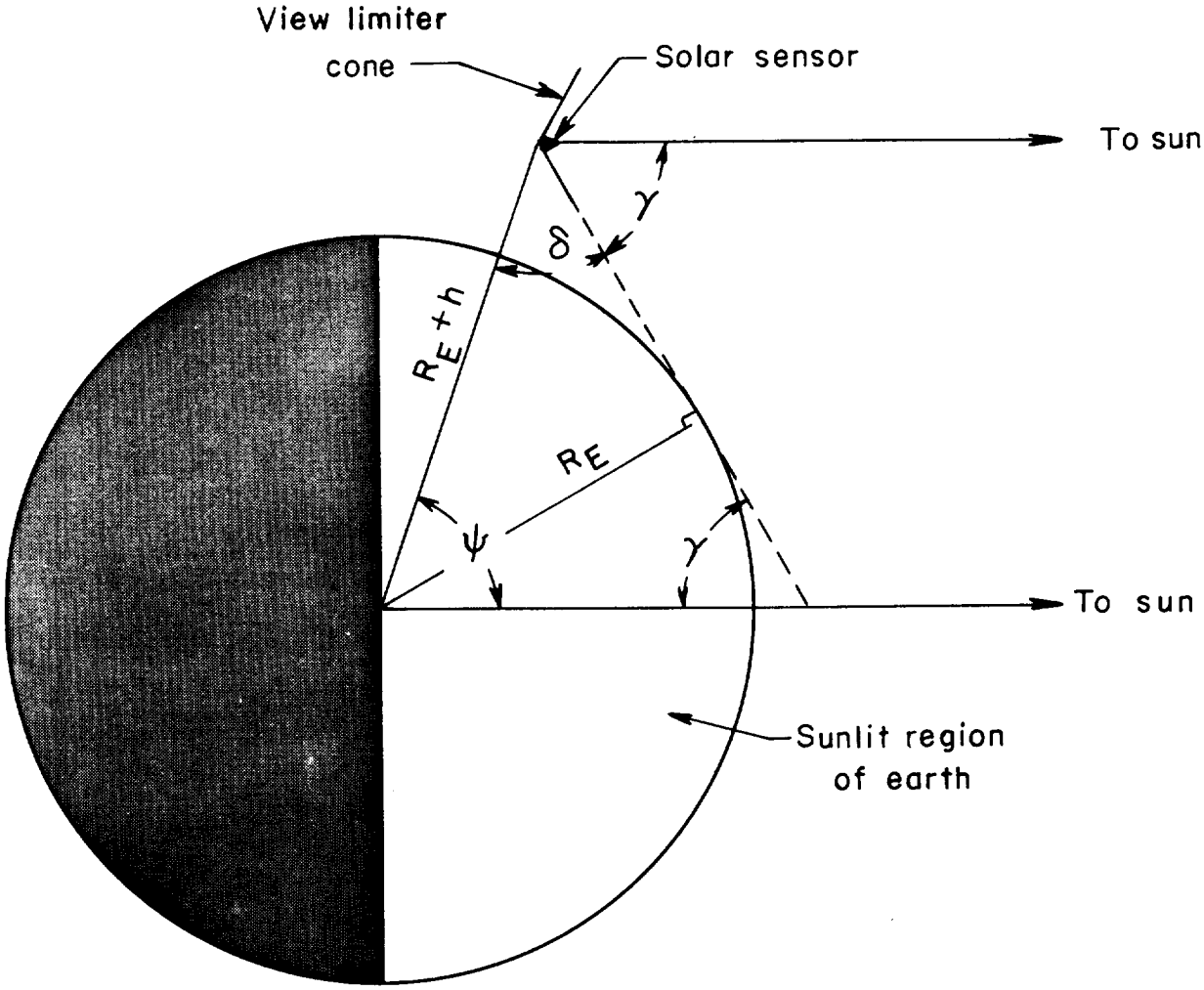

Figure 10.- Geometry of view limiter.

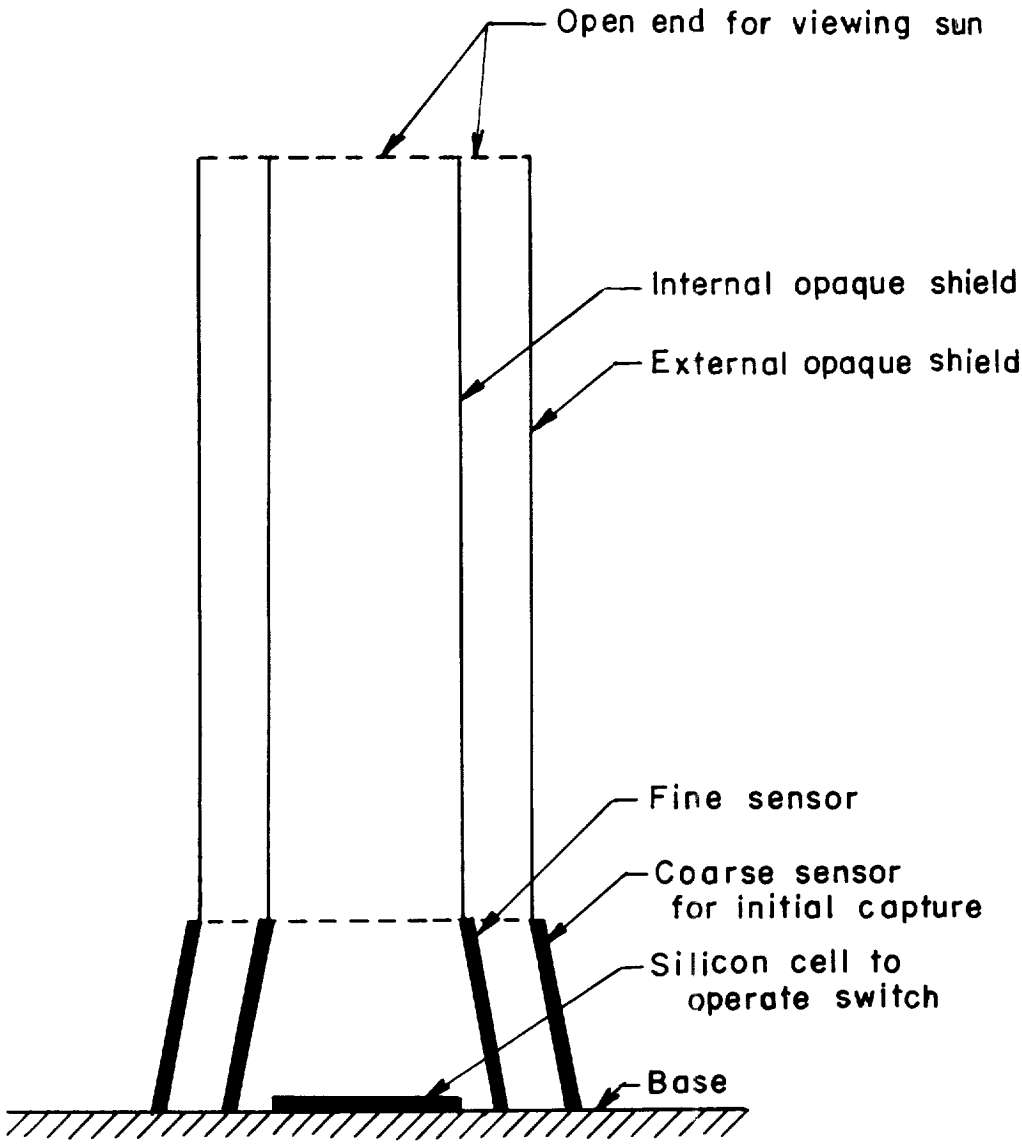

Figure 11.- Elimination of reflected-sunlight error.

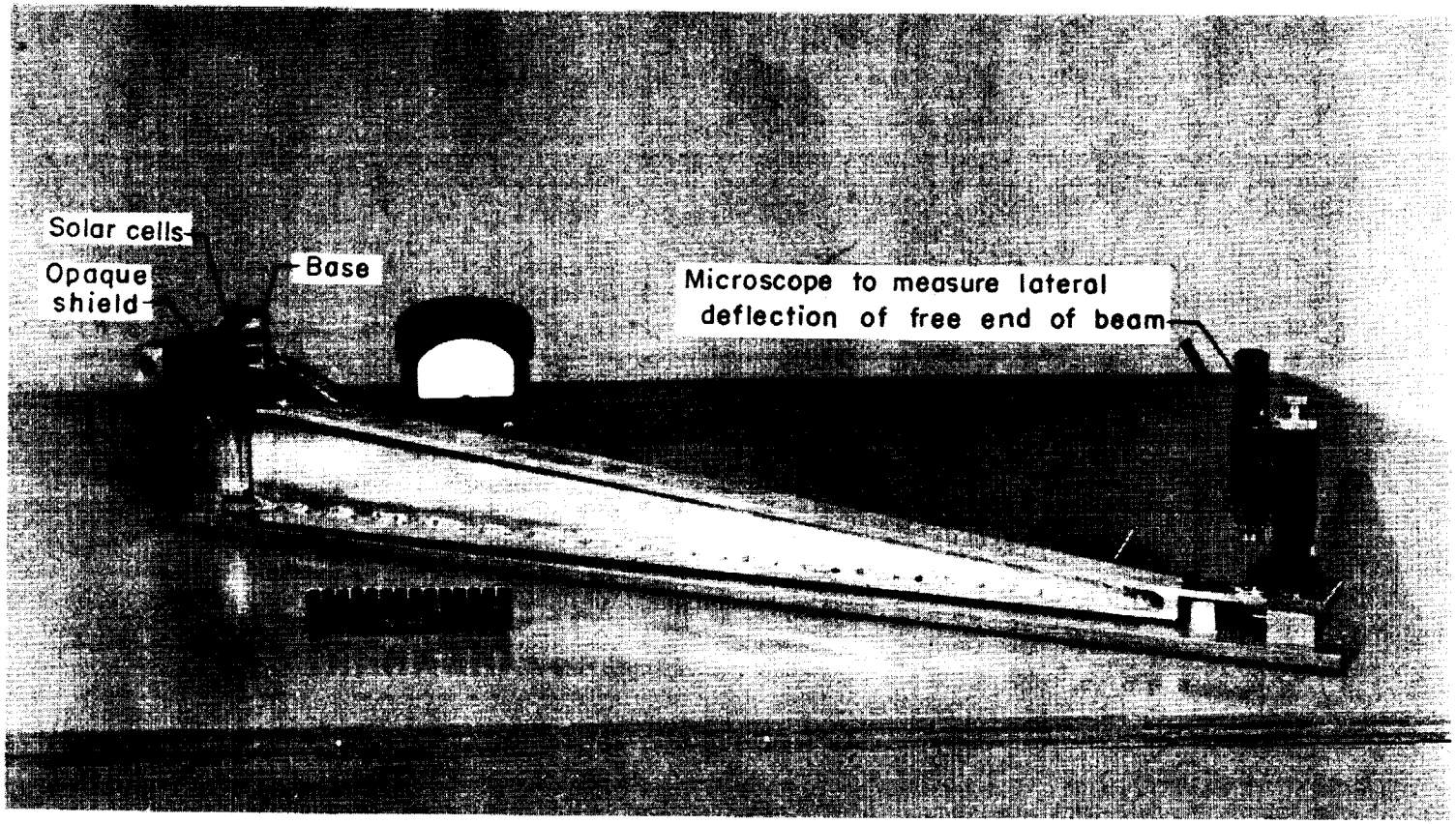

L-60-4664.1

Figure 12.- Experimental version of solar sensor attached to I-beam for small-angle calibration. Circular cells in shield provide a separate signal to sense angular velocity.

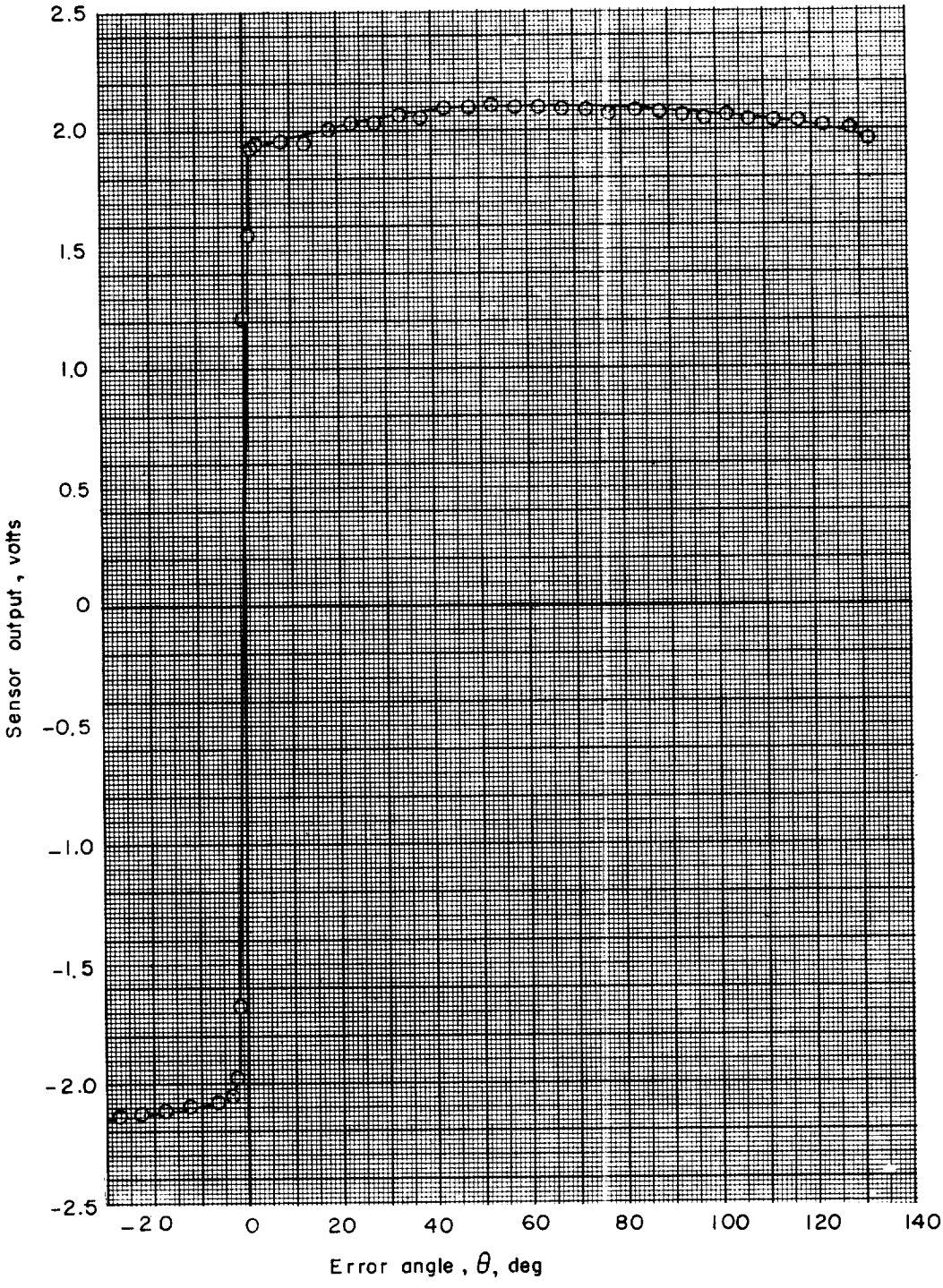

Figure 13.- Large-angle performance of experimental solar sensor.

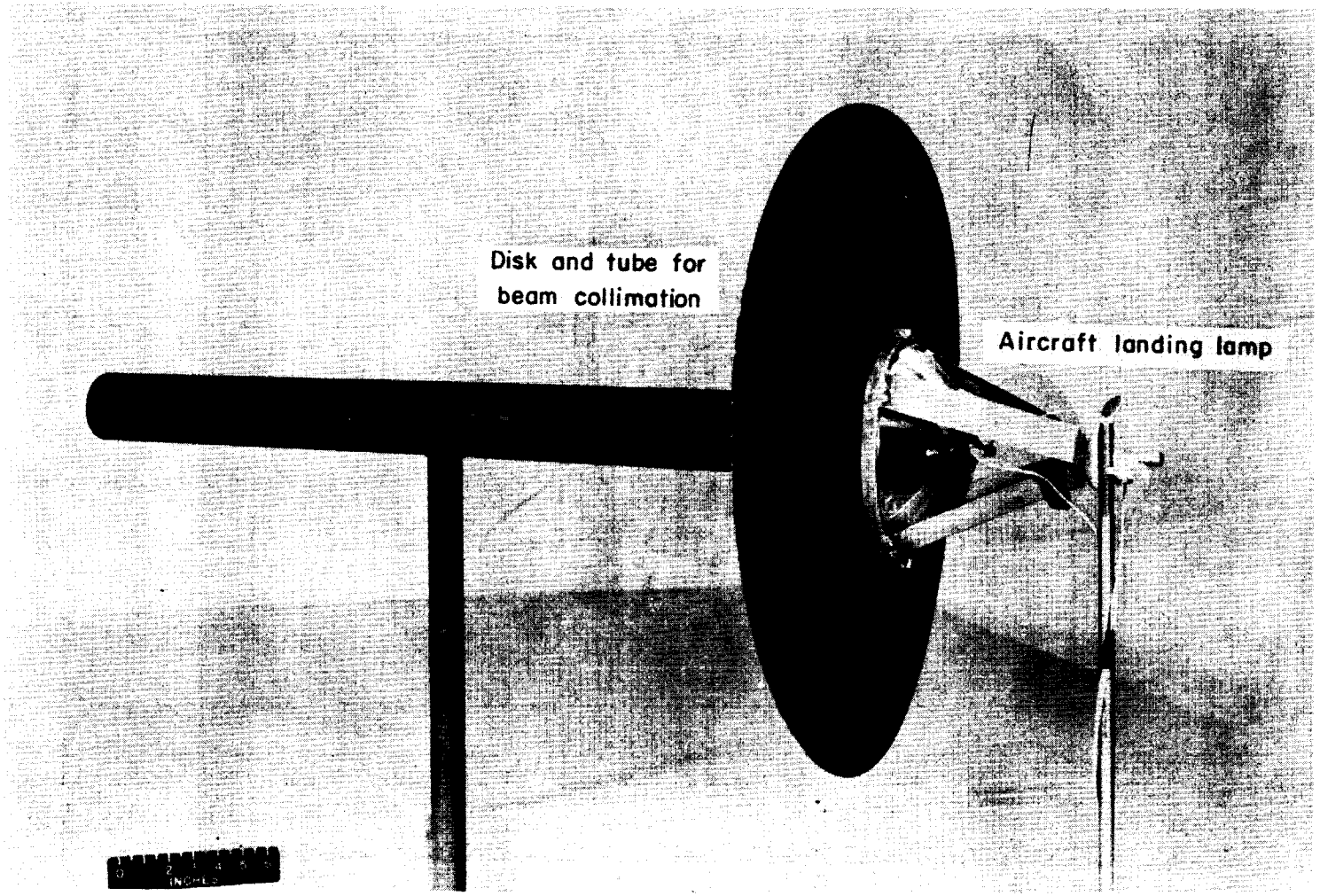

Figure 14.- Light source for solar sensor calibration. L-60-4663.1

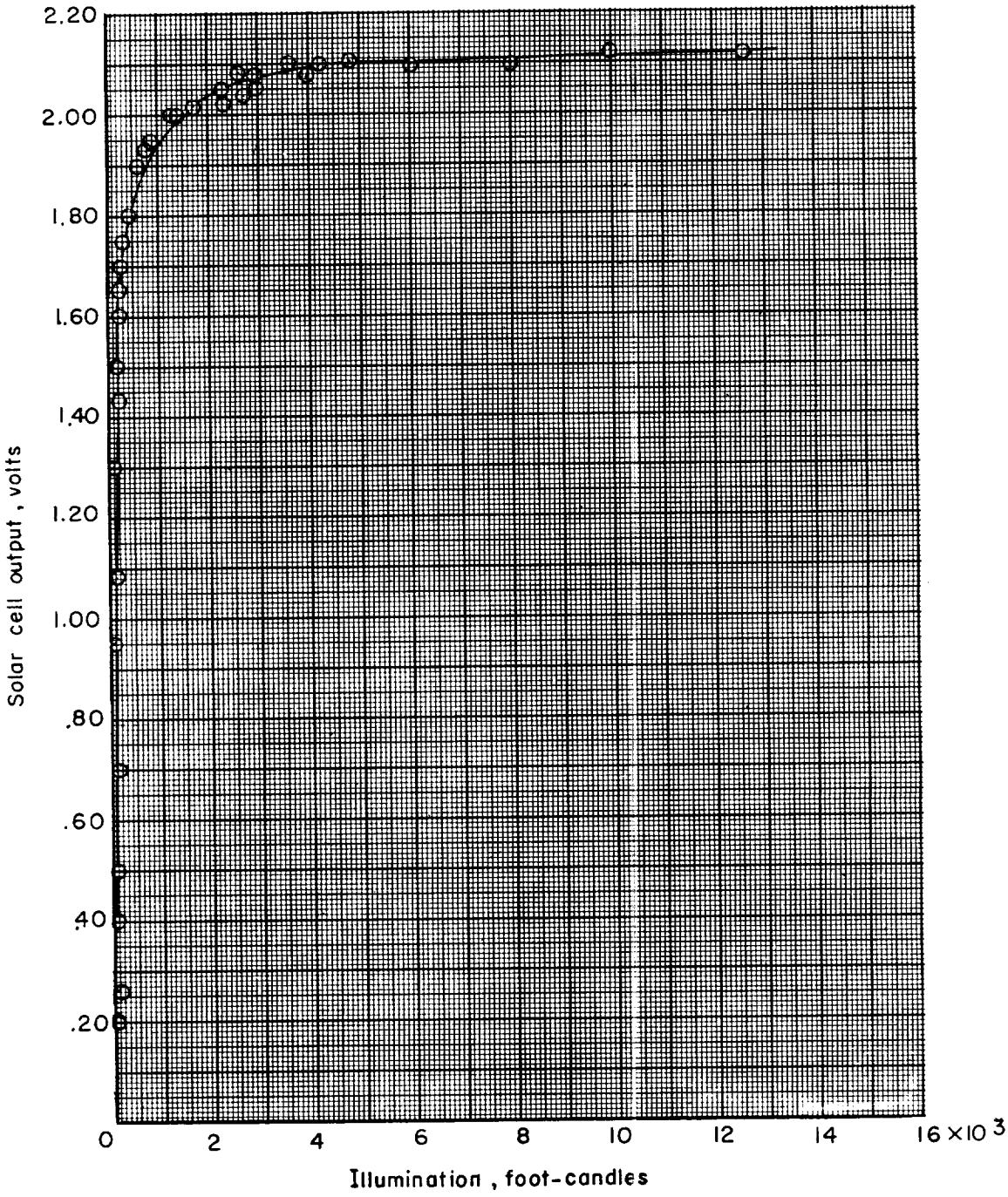

Figure 15.- Light saturation curve for one face of solar sensor. Load resistance, 1,000 ohms.

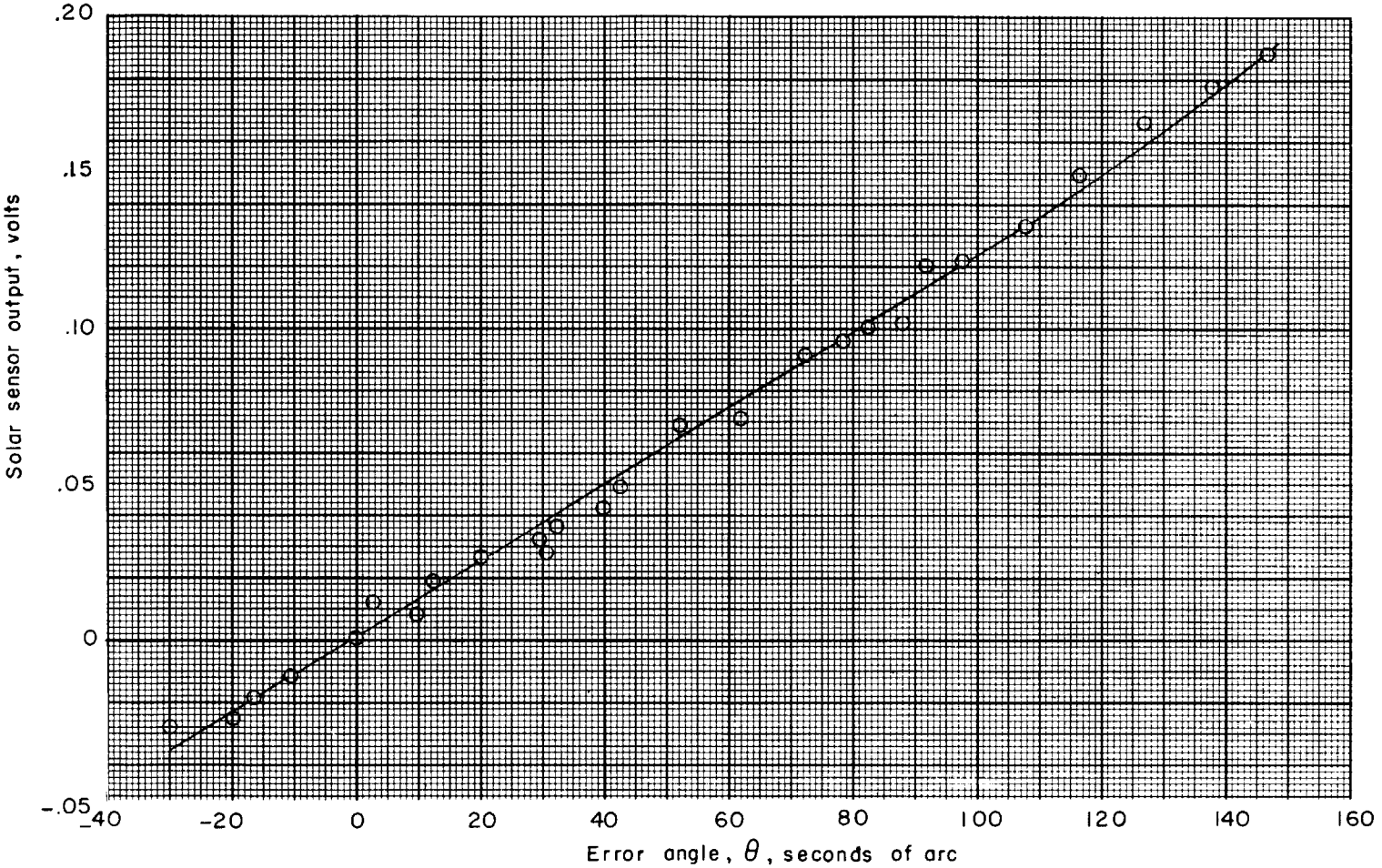

Figure 16.- Small-angle performance of experimental solar sensor. Source of illumination, 1,200-foot-candle aircraft landing lamp.

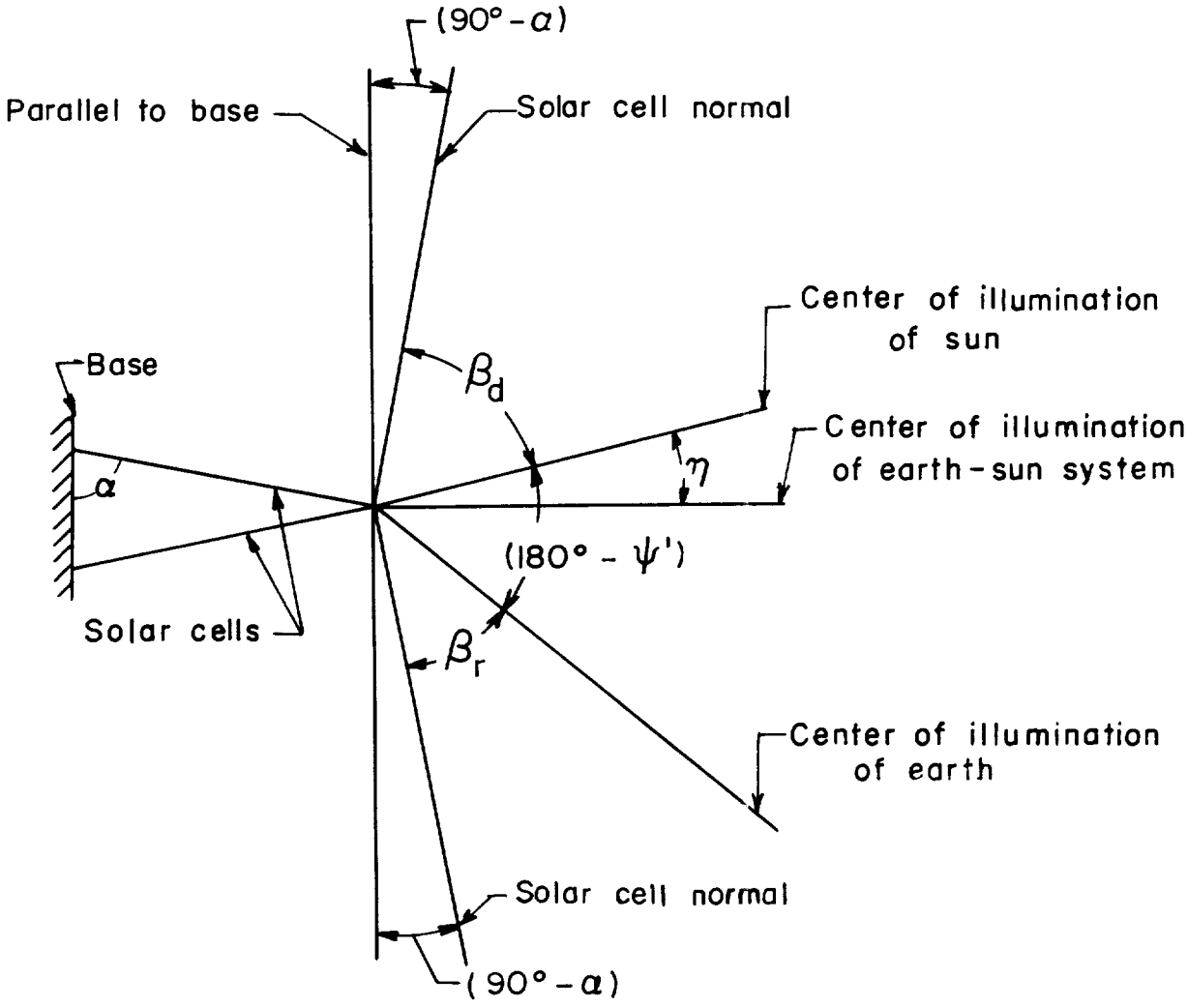

Figure 17.- Problem geometry.

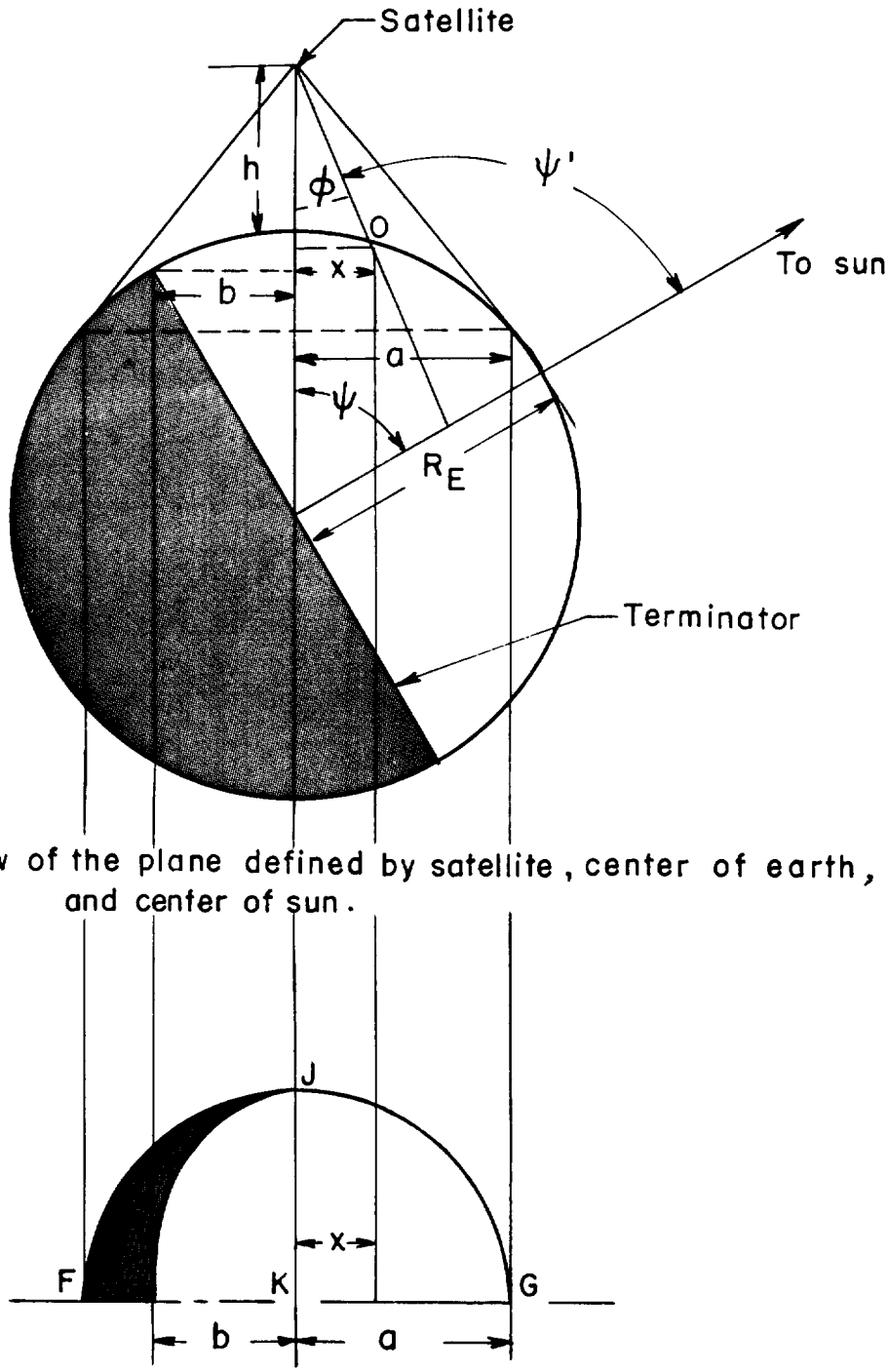

Figure 18.- Geometry of reflected earth radiation.

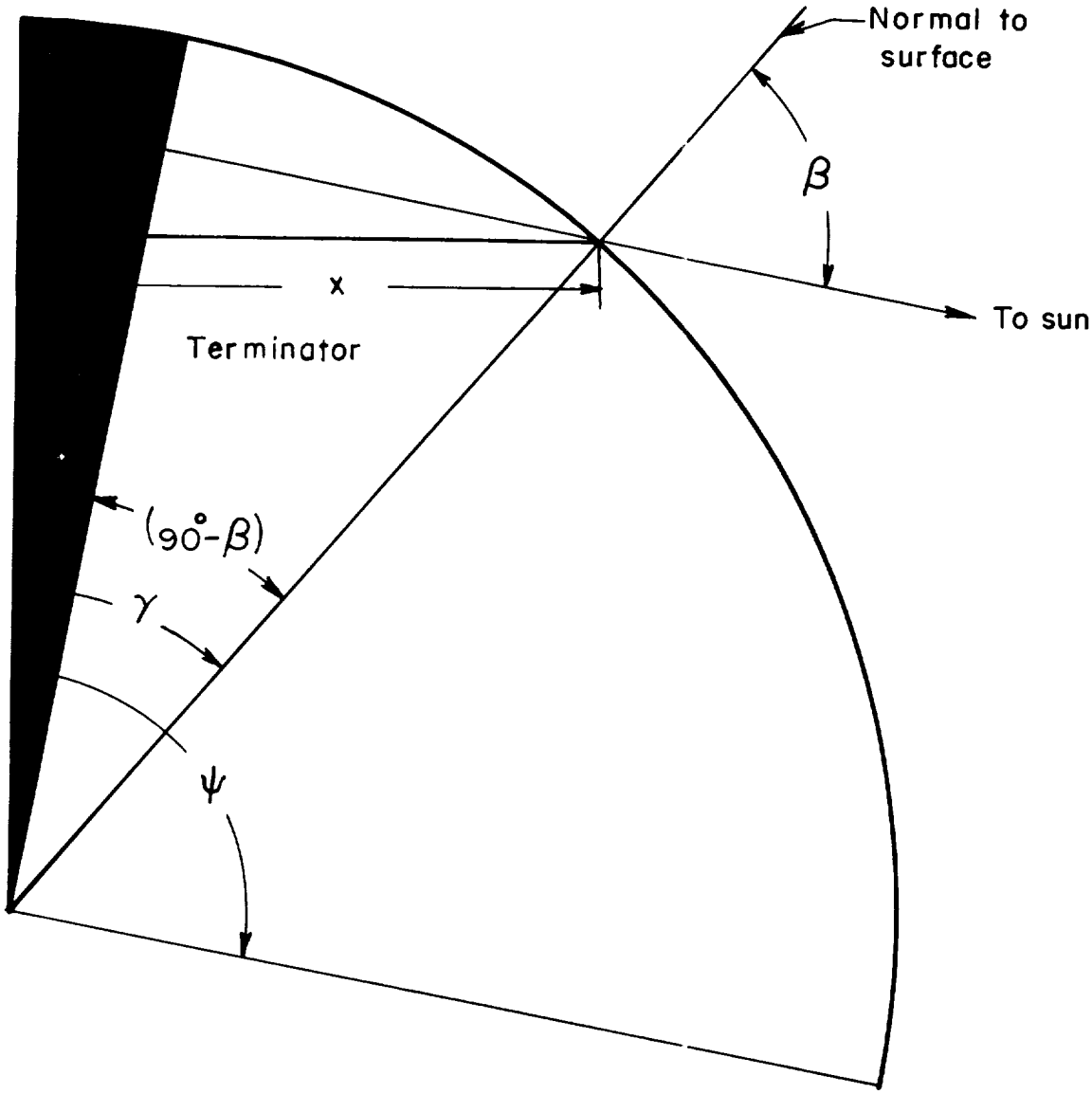

Figure 19.- Angle of incidence for the most general case.

L-1308

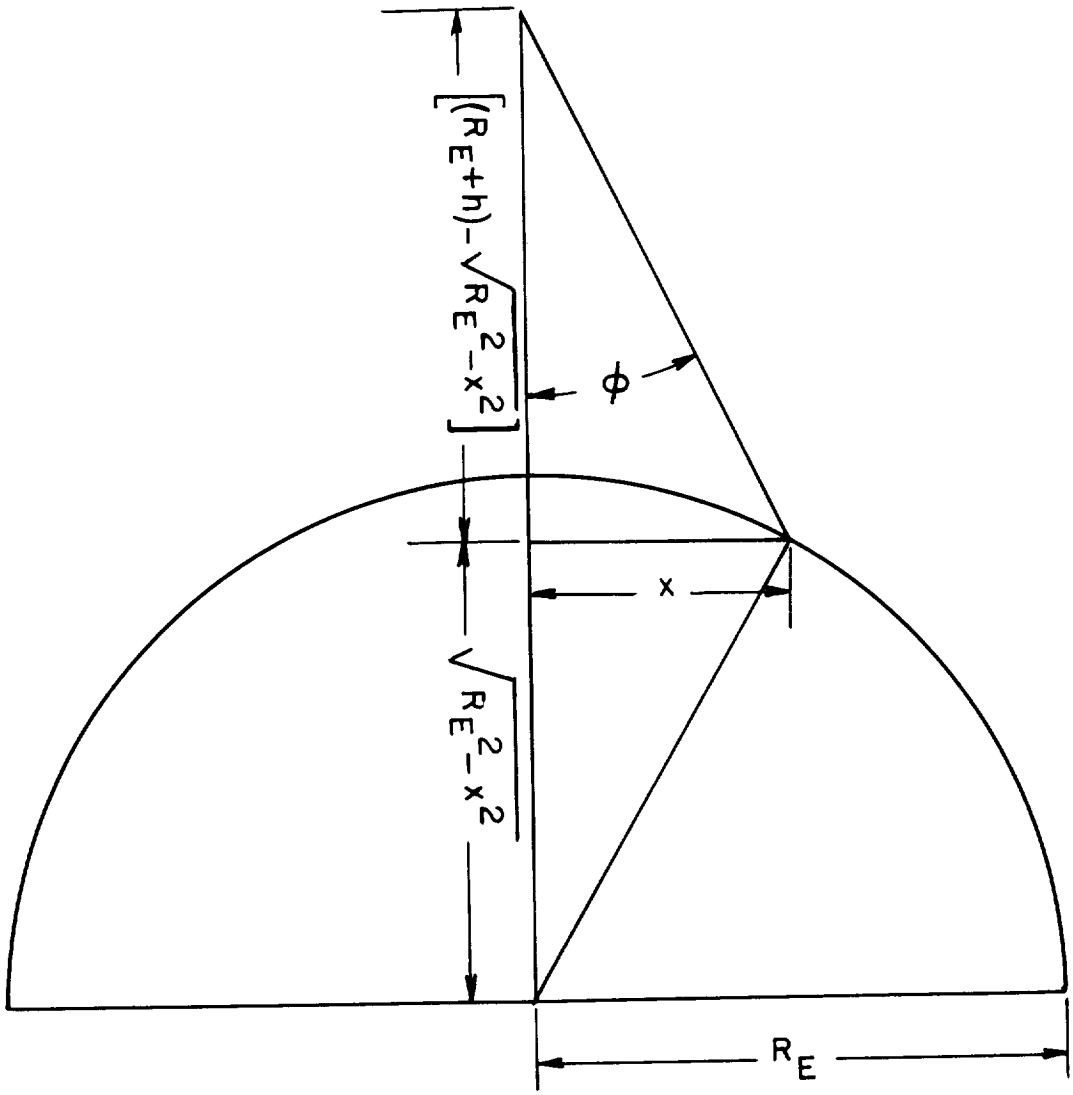

Figure 20.- Geometry used to determine ϕ.